

Identifying Minimal Composite Dark Matter

Shuai Xu* and Sibozheng†

*Department of Physics,
Chongqing University,
Chongqing 401331, China*

Abstract

We attempt to identify the minimal composite scalar dark matter from strong dynamics with the characteristic mass of order TeV scale. We provide both direct and indirect limits from dark matter direct detections and collider facilities. Compared to a fundamental scalar dark matter, our results show that in the composite scalar dark matter the disappearing resonant mass region, the smaller spin-independent dark matter-nucleon scattering cross section in certain mass region, and the absence at the HL-LHC illustrate how to differentiate these two dark matter models.

arXiv:2008.00173v1 [hep-ph] 1 Aug 2020

* shuaxu@cqu.edu.cn

† sibozheng.zju@gmail.com

I. INTRODUCTION

Although a Higgs-like boson [1, 2] in the standard model has been established by the LHC, there is still a lack of enough information about the “nature” of the observed Higgs. Whether it is a fundamental or a composite state is critical as it points to totally different new physics respect to the electroweak symmetry breaking. This question will be addressed by near future precision measurements on the Higgs at HL-LHC [3]. Similarly, there are also different choices on the thermal dark matter (DM), which can be either fundamental or composite. Since both the observed Higgs and yet confirmed DM are often simultaneously delivered by a single “dark” sector behind the electroweak symmetry breaking, instead of conventional choice [4] in this paper we will explore both a composite Higgs and a composite scalar dark matter (CSDM).

In this scenario, the well-known hierarchy problem is solved by identifying both of these scalars as pseudo-Nambu-Goldstone (PNG) bosons [5–7] tied to some global symmetry. For reviews, see, e.g.[8, 9]. Following the spirit of simplicity, we consider the minimal CSDM with the following features.

- The minimal structure of the coset which is suitable for both composite Higgs h and CSDM η is $SO(6)/SO(5)$ [10] based on the minimal composite Higgs model [11].
- The minimal matter content in the effective theory of the composite sector contains only the light composite Higgs and CSDM, with the other freedoms therein decoupled.
- The minimal representation of the composite fermions corresponds to the fundamental representation of $SO(6)$.

The features above yield the following effective Lagrangian¹ for the PNGBs in the minimal CSDM model

$$\begin{aligned} \mathcal{L}_{\text{eff}} = & \frac{1}{2} (\partial_\mu h)^2 - \frac{1}{2} m_h^2 h^2 - \frac{\lambda_{h^3}}{2} v h^3 - \frac{\lambda_{h^4}}{4} h^4 + \frac{1}{2} (\partial_\mu \eta)^2 - \frac{1}{2} m_\eta^2 \eta^2 - \frac{\lambda_{\eta^4}}{4} \eta^4 \\ & + \mathcal{L}_f + \mathcal{L}_V - \mathcal{L}_h + \dots, \end{aligned} \quad (1)$$

with

$$\mathcal{L}_h = \frac{\kappa_1}{2} v h \eta^2 + \frac{\kappa_2}{4} h^2 \eta^2 - (\partial_\mu h \partial^\mu \eta) \left[\frac{\xi}{\sqrt{1-\xi}} \frac{\eta}{v} + \frac{\xi(1+\xi)}{1-\xi} \frac{h\eta}{v^2} \right] - \frac{\xi^2}{1-\xi} (\partial_\mu h)^2 \frac{\eta^2}{v^2}, \quad (2)$$

$$\mathcal{L}_f = -m_\psi \bar{\psi} \psi \left[1 + \frac{1-2\xi}{\sqrt{1-\xi}} \frac{h}{v} - \frac{(3-2\xi)\xi}{2(1-\xi)} \frac{h^2}{v^2} - \frac{\xi}{2(1-\xi)} \frac{\eta^2}{v^2} \right], \quad (3)$$

$$\mathcal{L}_V = \left(m_W^2 W_\mu^+ W^{-\mu} + \frac{m_Z^2}{2} Z_\mu Z^\mu \right) \left[1 + 2\sqrt{1-\xi} \frac{h}{v} + (1-\xi) \frac{h^2}{v^2} \right], \quad (4)$$

where the constrained parametrization [14, 15] has been adopted, the Higgs mass $m_h = 125$ GeV, m_η is the CSDM mass, and $\xi = v^2/f^2$ with the weak scale $v = 246$ GeV and f referring

¹ Firstly, we use the Goldstone matrix to describe the PNGBs, then derive the kinetical terms in terms of Callan-Coleman-Wess-Zumino (CCWZ) formalism [12, 13], and finally calculate the Yukawa interactions between the PNGBs and SM fermions and the effective potential by using the spurion method (see, e.g.[8]).

to the breaking scale of $SO(6)$. We have neglected the next-to-leading-order terms as well as the derivative self interactions of the composite Higgs. Apart from the self interaction for η , which is actually decoupled from both the DM relic abundance constraint and DM direction detections, there are only three free parameters in Eqs.(1)-(4), as composed of the CSDM mass m_η , the Yukawa coupling² $\kappa = \kappa_1 \approx \kappa_2$ between η and Higgs, and the composite mass scale f or equivalently ξ , which are responsible for phenomenologies of the minimal CSDM. Although this observation is made in the constrained parametrization, it is also true in the other parameterizations, see e.g. [15].

We find that most of materials related to the minimal CSDM in the literature are either out of date or inadequate. For example, there are no updates on the parameter space subject to state-of-the-art DM direct detection limits. Moreover, the latest precision tests on the Higgs at the LHC are able to place strong indirect constraint on the parameter space. Finally, the direct collider detection on the CSDM at the LHC is nearly absent. We will attempt to address these questions in this paper. The rest of this paper is organized as follows. In Sec.II, we analyze the direct constraints on the CSDM from DM direct detection. Then, in Sec. III we turn to indirect constraints both from DM and collider experiments. Sec.IV is devoted to the direct probes of CSDM at the LHC. During the study, we will point out the important differences between the CSDM and the fundamental scalar dark matter (FSDM) [16, 17] (for review, see e.g.[18]). We present the final results and conclude in Sec.V.

II. DM PHENOMENOLOGY

A. Parameter Space Of Dark Matter

Instead of fixing κ as in ref.[15], which results from certain specific assumptions on the composite fermions in the composite sector, we take it as a free parameter with rational values. A relaxation on the parameter κ gives rise to a parameter space of thermal DM obviously larger than that in ref.[15].

Apart from a partial of interactions similar to that of FSDM [18, 19] in Eq.(2), \mathcal{L}_h also contains the derivative interactions with momentum dependence, which lead to significant deviation from the FSDM for f of order TeV scale. The derivative interactions contribute to $\eta\eta$ annihilation cross section in the manner that it grows as the DM mass increases, which can be interpreted from the modifications to the effective couplings in Eq.(2):

$$\begin{aligned}\kappa_1 &\approx \kappa - 2\xi \left(\frac{m_\eta^2}{v^2} \right) + \mathcal{O}(\xi^2), \\ \kappa_2 &\approx \kappa - 8\xi \left(\frac{m_\eta^2}{v^2} \right) + \mathcal{O}(\xi^2).\end{aligned}\tag{5}$$

In Eq.(5), the deviations are small in the limit $f \rightarrow \infty$, which corresponds to the FSDM as shown by the black curve in Fig.1. In contrast, the deviation is expected to be large in the

² In Eq.(2), κ_1 and κ_2 are identical up to $\mathcal{O}(\xi)$.

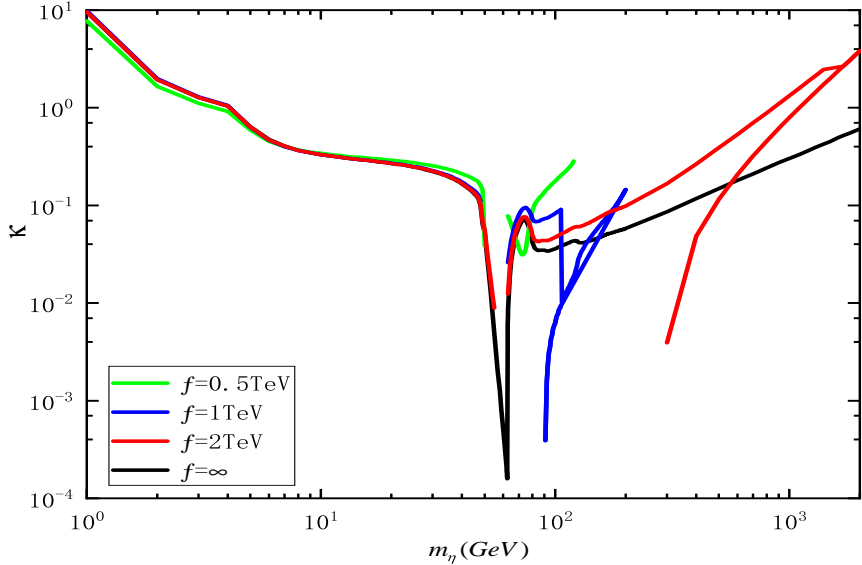


FIG. 1. Contours of thermal DM relic density projected to the two-parameter plane of $m_\eta - \kappa$ for the representative scales $f/\text{TeV} = 0.5$ (green), 1 (blue) and 2 (red), where the black curve refers to the FSDM with $f = \infty$.

case of small f , under which κ shifts from the value κ_\star [18, 19] referring to the FSDM as

$$\kappa \approx \left| \left(\frac{2m_\eta^2}{v^2} \right) \xi \pm \kappa_\star \right| \quad (6)$$

Fig.1 shows the parameter space respect to the thermal DM relic abundance $\Omega h^2 = 0.12 \pm 0.001$ [20] in terms of micrOMEGAs [21]. It reveals that compared to the FSDM, in the large CSDM mass region with $m_\eta \sim v$, Eq.(6) explains the distributions of various curves with ξ of order $\sim 0.01 - 0.2$ therein; while in the CSDM mass region with $m_\eta \sim m_h/2$, the well-known resonant mass window gradually disappears as f approaches to smaller value; and finally in the small CSDM mass $m_\eta \ll v$, κ in Eq.(6) approaches to κ_\star so that all the curves nearly overlap with that of FSDM.

In our discussion above, we have neglected the contribution to the $\eta\eta$ annihilation cross section from the contact interaction in Eq.(3), which is given by,

$$\sigma(\eta\eta \rightarrow \bar{\psi}\psi)v_{\text{rel}} \approx \frac{\xi^2}{16\pi} \frac{m_\psi^2}{v^4} \left(1 - \frac{m_\psi^2}{m_\eta^2} \right)^{3/2}. \quad (7)$$

Because of the fermion mass suppression in Eq.(7), the contribution can be indeed ignored in the CSDM mass range $m_\eta < m_t$. Even for the CSDM mass range $m_\eta > m_t$ as covered by the case with $f = 2$ TeV in Fig.1, $\sigma(\eta\eta \rightarrow \bar{t}t)v_{\text{rel}}$ is small compared to the inferred value $\langle \sigma v_{\text{rel}} \rangle \sim 3 \times 10^{-26} \text{cm}^3 \text{s}^{-1}$, which indicates that the previous estimate on the behavior of this curve is still valid.

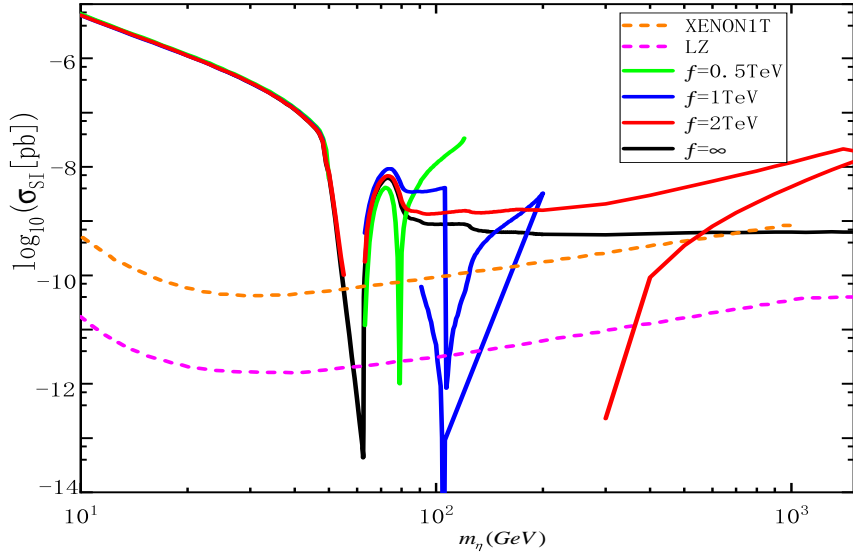


FIG. 2. SI cross section as function of m_η for the representative scales as in Fig.1, which reveals that in certain CSDM mass range between 63 GeV and 600 GeV an improved XENON1T or future LZ results are useful in discriminating the CSDM from the FSDM.

B. Direct Detection

The spin-independent (SI) scattering cross section for the CSDM relies on both the CSDM mass and the effective coupling for the $\eta - \eta - h$ vertex, which reads as

$$\sigma_{\text{SI}} \approx \frac{\kappa^2 f_N^2 \mu^2 m_N^2}{4\pi m_h^4 m_\eta^2}, \quad (8)$$

where m_N is the nucleon mass, $\mu = m_\eta m_N / (m_\eta + m_N)$ is the DM-nucleon reduced mass, and $f_N \approx 0.3$ is the hadron matrix element. Unlike the effective couplings in the preceding analysis on the DM relic abundance, the corrections to the effective coupling κ in Eq.(8) due to the derivative interactions are negligible.

Fig.2 explicitly shows the numerical results about the SI cross sections extracted from the DM parameter space in Fig.1. In this figure, one finds that unlike the FSDM, in which DM mass below ~ 700 GeV is nearly excluded by the latest XENON1T limit [22], a large part of the CSDM mass window between ~ 63 GeV and ~ 600 GeV is still beneath the latest XENON1T limit [22] and can be in the reach of future LZ experiment [23]. This means that *the future XENON1T or LZ results in this mass window can be useful in discriminating the CSDM from the FSDM.*

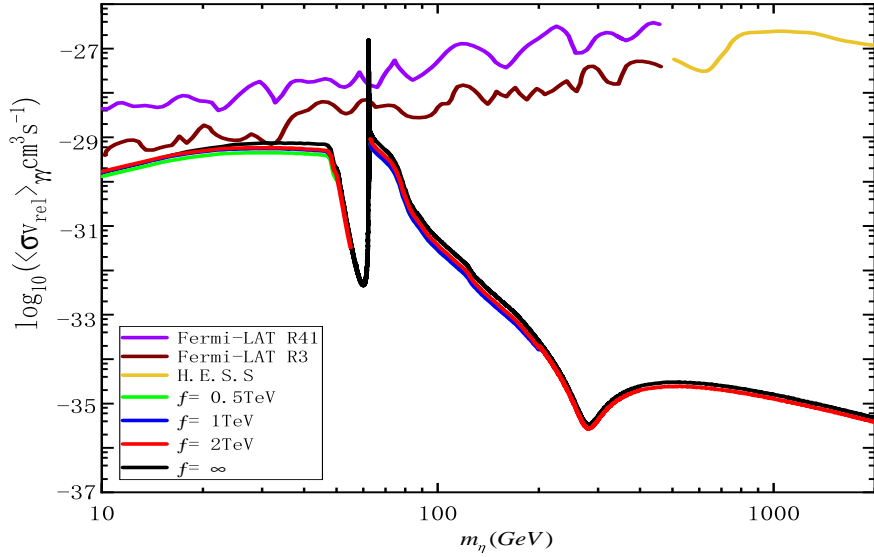


FIG. 3. The averaged cross section $\langle \sigma_{\gamma\gamma} v_{\text{rel}} \rangle$ for various scales f as in Fig.1. Compared to the FSDM, the indirect constraint on the CSDM from γ ray is slightly weaker.

III. INDIRECT CONSTRAINTS

A. Gamma Ray

Astrophysical observation of gamma ray is an important experiment to indirectly constrain the thermal DM. The value of $\langle \sigma_{\gamma\gamma} v_{\text{rel}} \rangle$ can be calculated via the standard formula [24],

$$\langle \sigma_{\gamma\gamma} v_{\text{rel}} \rangle = \frac{x}{16m_\eta^5 K_2^2(x)} \int_{4m_\eta^2}^{\infty} ds \sqrt{s - 4m_\eta^2} s K_1 \left(\frac{x\sqrt{s}}{m_\eta} \right) \sigma_{\gamma\gamma} v_{\text{rel}}, \quad (9)$$

where $x = m_\eta/T$, s is the square of the center-of-mass energy, and K_1 and K_2 are modified Bessel functions of the second kind. In Eq.(9), the annihilation cross section reads as,

$$\sigma_{\gamma\gamma} v_{\text{rel}} = \frac{2v^2}{\sqrt{s}} \left(\kappa - \frac{2m_\eta^2}{v^2} \xi \right)^2 \frac{\Gamma_{h \rightarrow \gamma\gamma}}{(s - m_h^2)^2 + m_h^2 \Gamma_h^2}, \quad (10)$$

where $\Gamma_h \approx 4.15$ MeV is the total decay width for the SM-like Higgs, and $\Gamma_{h \rightarrow \gamma\gamma}$ is mainly determined by two types of one-loop Feynman diagrams with either virtual vector bosons or fermions [25], whose couplings to the Higgs are corrected by factor $(1 - 2\xi)/\sqrt{1 - \xi}$ and $\sqrt{1 - \xi}$, respectively.

Substituting the correlated values of m_η and κ in Fig.1 into Eq.(9), we show in Fig.3 the numerical results of $\langle \sigma_{\gamma\gamma} v_{\text{rel}} \rangle$ for the representative values of f in Fig.1, where the Fermi-LAT [26, 27] and HESS [28] limits are shown simultaneously. Compared to the FSDM, the

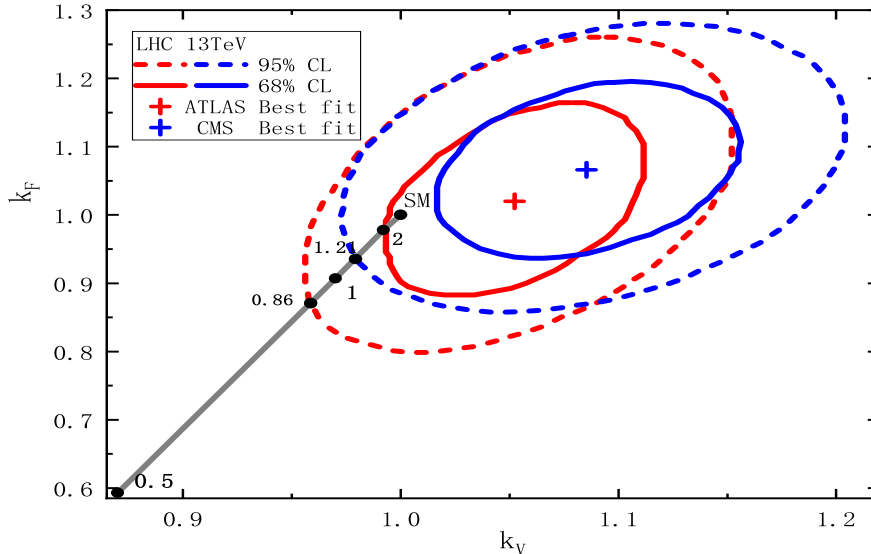


FIG. 4. The Higgs couplings for the representative values of f in Fig.1, where both the 68% and 95% contours of the best fits values of k_F and k_V are shown for comparison and the values of f at the crossing points are explicitly shown. We have taken the best fits to these Yukawa coupling constants reported in [29, 30].

values of $\langle\sigma_{\gamma\gamma}v_{\text{rel}}\rangle$ in the case of CSDM are slightly smaller as a result of the suppressions on the Higgs couplings as mentioned above.

B. Precision Test On Higgs Couplings

The precision measurements on the Higgs couplings are able to effectively constrain the parameter range of f . According to the features of the composite Higgs couplings in Eqs.(3)-(4), we use the conventional two-parametrization fit for our analysis, under which we have

$$k_V = \sqrt{1 - \xi}, \quad k_F = \frac{1 - 2\xi}{\sqrt{1 - \xi}}. \quad (11)$$

Fig.4 shows the constraint on f from the latest 13-TeV LHC data, where the ATLAS best fits are given by $k_V = 1.05$ and $k_F = 1.05$ [29] and the CMS best fits are given by $k_V = 1.08$ and $k_F = 1.06$ [30] respectively. This figure indicates that the latest ATLAS and CMS results have excluded the parameter range $f < 0.86$ TeV and $f < 1.21$ TeV at 95% CL, respectively. These lower bounds will be significantly improved at the future LHC, which makes the precision tests on the Higgs couplings more competitive³ than the precision measurements on the electroweak observables [31]. In what follows, we will not discuss the case with $f = 500$ GeV.

³ Although strong, this indirect constraint may be however evaded in the situation with either non-minimal matter content or non-fundamental representation for the composite fermions.

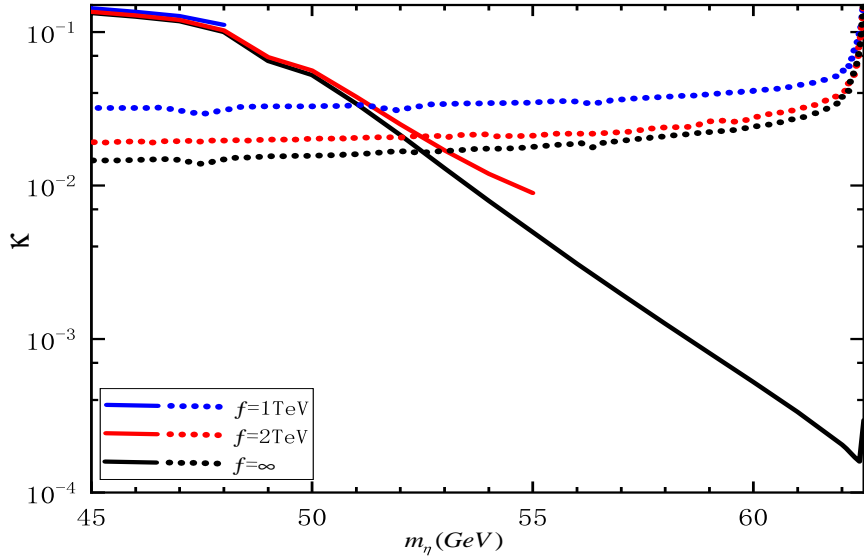


FIG. 5. Same as Fig.1 with the contours of Higgs invisible decay width $\text{Br}(h \rightarrow \eta\eta) = 16\%$ [32] (in dotted), above which the CSDM mass region is excluded.

C. Precision Test On Higgs Decay

In the CSDM mass region with $m_\eta < m_h/2$, the composite Higgs can directly decay into the η pair either via the Higgs portal interactions in Eq.(2) or the contact interactions in Eq.(3). The derivative interactions in Eq.(2) result in a modification to the effective coupling in the Higgs invisible decay, while the contact interactions contribute to Higgs invisible decay through the top-, W - and Z -loop induced processes. All of the loop effects are controlled by the magnitude of ξ . Without the loop effect, the decay width is approximated as

$$\Gamma(h \rightarrow \eta\eta) \approx \frac{v^2}{32\pi m_h} \left(\kappa - \frac{2m_h^2}{v^2} \xi \right)^2 \sqrt{1 - \frac{4m_\eta^2}{m_h^2}}. \quad (12)$$

We show in Fig.5 the contours of the latest experimental bound on the Higgs invisible decay width $\text{Br}(h \rightarrow \eta\eta) \leq 16\%$ [32] for the representative values of f as in Fig.1, above which the CSDM mass region is excluded. Compared to the constraint in the FSDM, the others are slightly weaker. The reason for this is due to a mild cancellation between the Yukawa and derivative interactions in Eq.(12) given nearly the same κ in the mass region $m_\eta < m_h/2$ regardless of the value of f , see Eq.(1). As a result, the constraint from the Higgs invisible decay is relaxed for finite f . Nevertheless, the absence of the resonant mass region for small f makes this relaxation useless.

The observation holds even with the loop effects taken into account. For example, the top-loop induced contribution modifies κ in Eq.(12) by a factor $\sim \xi \left(\frac{m_t}{v}\right)^3 \log\left(\frac{m_t}{\mu}\right)$, with μ a cut-off scale. For f larger than 1 TeV, it is obviously smaller than κ .

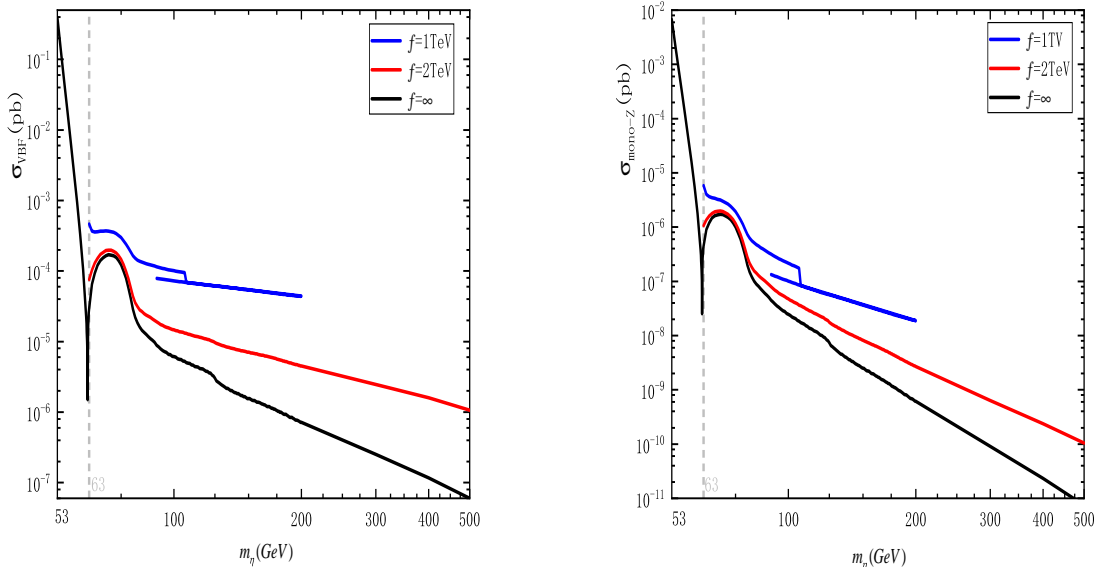


FIG. 6. Cross sections of the VBF (left) and mono-Z (right) process at the 14 TeV LHC for the values of f as in Fig.1, respectively.

IV. DIRECT DETECTION AT LHC

In this section, we turn to the direct production of the CSDM pair at the LHC. To calculate the numbers of events of relevant signals and their SM backgrounds, we use FeynRules [33] to generate model files prepared for MadGraph5 [34] that includes Pythia 6 [35] for parton showering & hadronization, and Delphes 3 [36] for fast detector simulation. The leading-order events are obtained in terms of MadGraph5 by extracting samples from the CSDM parameter space in Fig.1.

From the Higgs portal in Eq.(2), the η pair production at the LHC is similar to that of FSDM. The discovery channels mainly include the vector boson fusion (VBF) process

$$pp \rightarrow jjh^* \rightarrow jj\eta\eta, \quad (13)$$

and the mono-Z process

$$pp \rightarrow Zh^* \rightarrow Z\eta\eta, \quad (14)$$

where h is virtual for $m_\eta > m_h/2$, and the two jets in Eq.(13) can be either the same or different. These processes have been used to derive the prospect of the resonant mass region $m_\eta \sim m_h/2$ at the LHC for the FSDM [37–39]. Unlike the FSDM, the main contribution to the production cross sections of these two signal channels at the 14 TeV LHC is dominated by the derivative interactions. Although the derivative interactions enhance the production cross sections, as illustrated in Fig.6, compared to their SM backgrounds they are about at least six orders of magnitude smaller. So large gap between the cross sections of these

signals and their SM backgrounds makes them unlikely to constrain the CSDM at the HL-LHC with an integrated luminosity as high as 3000 fb^{-1} . We draw this conclusion based on the 13-TeV CMS cuts reported in [40] and [41] for the VBF and mono-Z respectively.

In addition, the contact interactions in Eq.(3) provide alternative production processes different from those of FSDM. Among them, the top-loop induced gluon gluon fusion (GGF) process⁴

$$pp \rightarrow jj\eta\eta, \quad (15)$$

has the largest signal rate. Besides the GGF process, there are also signal channels with top quark pair such as $pp \rightarrow \bar{t}t\eta\eta \rightarrow \bar{b}bjjj\eta\eta$ with hadronic final states and $pp \rightarrow \bar{t}t\eta\eta \rightarrow \bar{b}bjjj\eta\ell\nu$ with leptonic final state(s) [42], whose SM backgrounds are mainly given by $pp \rightarrow \bar{b}bjjj\nu\nu$ and $pp \rightarrow \bar{b}bjj\ell\nu$, respectively. The GGF process has the cross section of order up to $\sim 10^2 \text{ fb}$, while the processes with the top quark pairs have cross section of order up to $\sim 10^{-1} \text{ fb}$. Unfortunately, all of these production cross sections are too small. Take the GGF process for example. Compared to its SM background with the cross section of order $\sim 6 \times 10^4 \text{ pb}$, the GGF process fails to provide any useful constraint, no matter how the selection of events are performed.

Based on the null results from the VBF, mono-Z and GGF processes, the minimal CSDM with mass $m_\eta > m_h/2$ is totally invisible at the high-luminosity(HL)-LHC with the integrated luminosity 3000 fb^{-1} . Consider that the CSDM couplings to the SM Higgs and fermions aren't obviously altered in the situation of non-minimal scenarios, we infer that the missing CSDM at the LHC is probably a general result.

V. CONCLUSIONS

In this paper, we have made a comprehensive investigation on the CSDM in the minimal setup. Although totally different from the FSDM, the CSDM mimics the FSDM when the scale of global symmetry breaking f is far than the weak scale. But their differences become “visible” as f decreases to the order of TeV scale (where the fine tuning is small). The minimal CSDM has been exposed by imposing both direct and indirect constraints. Fig.7 shows how to differentiate it from the FSDM as what follows.

- Disappearing resonant mass region. As seen from $f = \infty$ to $f = 1 \text{ TeV}$ in Fig.7, the resonant mass region gradually disappears.
- Small SI DM-nucleon scattering cross section in certain mass region. Instead of the exclusion mass bound larger than $\sim 700 \text{ GeV}$ in the FSDM, a large part of the CSDM mass window between $\sim 63 \text{ GeV}$ and $\sim 600 \text{ GeV}$ is still beneath the nowadays XENON1T limit. Since future XENON1T or LZ experiments can reach a partial of this mass region, they are very useful in discriminating the CSDM from the FSDM.

⁴ Concretely speaking, both the contact and Higgs interactions contribute to this GGF process, with the former dominating over the later.

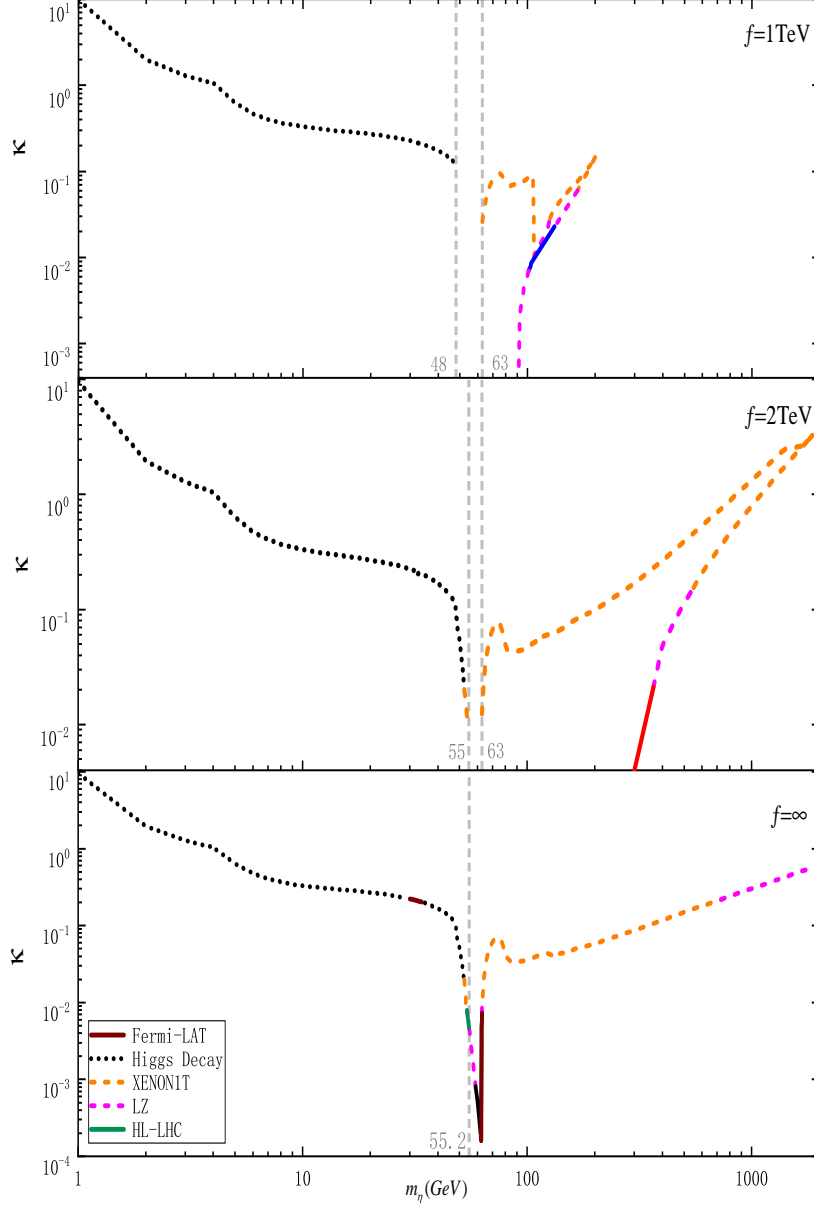


FIG. 7. The CSDM mass subject to the combination of direct detection (nowadays XENON1T and future LZ limits) as well as the indirect constraints from the γ ray (Fermi-LAT limit), the Higgs invisible decay and the precision tests on the Higgs couplings, where the conservative ATLAS bound $f > 0.86$ TeV at 95% CL has been taken. The FSDM (the lowest plot) is shown for comparison, where the 5σ discovery limit [39] at the HL-LHC is highlighted in dark green. The references of the other colors are the same as before.

- The absence of CSDM at the HL-LHC. Compared to certain signal reach near the resonant region in the FSDM as shown by the dark green curve in Fig.7, the absence of CSDM at the HL-LHC implies that similar to LZ, the HL-LHC can serve an alternative platform to differentiate these two DM models.

ACKNOWLEDGMENTS

Zheng would like to thank the Department of Physics at Harvard University for hospitality, where this work was initiated. The research is supported in part by the National Natural Science Foundation of China with Grant No. 11775039 and the Fundamental Research Funds for the Central Universities at Chongqing University with Grant No. cqu2017hbrc1B05.

-
- [1] G. Aad *et al.* [ATLAS], “Observation of a new particle in the search for the Standard Model Higgs boson with the ATLAS detector at the LHC,” *Phys. Lett. B* **716**, 1-29 (2012), [arXiv:1207.7214 [hep-ex]].
 - [2] S. Chatrchyan *et al.* [CMS], “Observation of a New Boson at a Mass of 125 GeV with the CMS Experiment at the LHC,” *Phys. Lett. B* **716**, 30-61 (2012), [arXiv:1207.7235 [hep-ex]].
 - [3] S. Dawson *et al.*, “Working Group Report: Higgs Boson,” [arXiv:1310.8361 [hep-ex]].
 - [4] S. Xu and S. Zheng, “Probing Electroweak Dark Matter at 14 TeV LHC,” [arXiv:1912.00404 [hep-ph]].
 - [5] D. B. Kaplan and H. Georgi, “SU(2) x U(1) Breaking by Vacuum Misalignment,” *Phys. Lett. B* **136**, 183 (1984).
 - [6] D. B. Kaplan, H. Georgi and S. Dimopoulos, “Composite Higgs Scalars,” *Phys. Lett. B* **136**, 187 (1984).
 - [7] M. J. Dugan, H. Georgi and D. B. Kaplan, “Anatomy of a Composite Higgs Model,” *Nucl. Phys. B* **254**, 299 (1985).
 - [8] G. Panico and A. Wulzer, “The Composite Nambu-Goldstone Higgs,” *Lect. Notes Phys.* **913**, pp.1-316 (2016), [arXiv:1506.01961 [hep-ph]].
 - [9] R. Contino, “The Higgs as a Composite Nambu-Goldstone Boson,” [arXiv:1005.4269 [hep-ph]].
 - [10] B. Gripaios, A. Pomarol, F. Riva and J. Serra, “Beyond the Minimal Composite Higgs Model,” *JHEP* **04**, 070 (2009), [arXiv:0902.1483 [hep-ph]].
 - [11] K. Agashe, R. Contino and A. Pomarol, “The Minimal composite Higgs model,” *Nucl. Phys. B* **719**, 165 (2005), [arXiv:hep-ph/0412089 [hep-ph]].
 - [12] S. R. Coleman, J. Wess, and B. Zumino, “Structure of phenomenological Lagrangians. 1.,” *Phys. Rev.* **177** (1969) 2239.
 - [13] J. Callan, Curtis G., S. R. Coleman, J. Wess and B. Zumino, “Structure of phenomenological Lagrangians. 2.,” *Phys. Rev.* **177** (1969) 2247.
 - [14] M. Frigerio, A. Pomarol, F. Riva and A. Urbano, “Composite Scalar Dark Matter,” *JHEP* **07**, 015 (2012), [arXiv:1204.2808 [hep-ph]].
 - [15] D. Marzocca and A. Urbano, “Composite Dark Matter and LHC Interplay,” *JHEP* **07**, 107 (2014), [arXiv:1404.7419 [hep-ph]].
 - [16] V. Silveira and A. Zee, “Scalar Phantoms,” *Phys. Lett. B* **161**, 136 (1985).
 - [17] J. McDonald, “Thermally generated gauge singlet scalars as self-interacting dark matter,” *Phys. Rev. Lett.* **88**, 091304 (2002), [hep-ph/0106249].

- [18] J. M. Cline, K. Kainulainen, P. Scott and C. Weniger, “Update on scalar singlet dark matter,” *Phys. Rev. D* **88** (2013) 055025, [arXiv:1306.4710 [hep-ph]].
- [19] H. Han and S. Zheng, “New Constraints on Higgs-portal Scalar Dark Matter,” *JHEP* **12**, 044 (2015), [arXiv:1509.01765 [hep-ph]].
- [20] N. Aghanim *et al.* [Planck], “Planck 2018 results. VI. Cosmological parameters,” [arXiv:1807.06209 [astro-ph.CO]].
- [21] G. Belanger, F. Boudjema, A. Pukhov and A. Semenov, “micrOMEGAs4.1: two dark matter candidates,” *Comput. Phys. Commun.* **192**, 322 (2015), [arXiv:1407.6129 [hep-ph]].
- [22] E. Aprile *et al.* [XENON Collaboration], “Dark Matter Search Results from a One Ton-Year Exposure of XENON1T,” *Phys. Rev. Lett.* **121**, no. 11, 111302 (2018), [arXiv:1805.12562 [astro-ph.CO]].
- [23] D. S. Akerib *et al.* [LUX-ZEPLIN Collaboration], “Projected WIMP Sensitivity of the LUX-ZEPLIN (LZ) Dark Matter Experiment,” [arXiv:1802.06039 [astro-ph.IM]].
- [24] P. Gondolo and G. Gelmini, “Cosmic abundances of stable particles: Improved analysis,” *Nucl. Phys. B* **360**, 145 (1991).
- [25] J. F. Gunion, H. E. Haber, G. L. Kane, and S. Dawson, *The Higgs Hunter’s Guide*, *Front. Phys.* **80** (2000) 1-448.
- [26] M. Ackermann *et al.* [Fermi-LAT Collaboration], “Updated search for spectral lines from Galactic dark matter interactions with pass 8 data from the Fermi Large Area Telescope,” *Phys. Rev. D* **91**, no. 12, 122002 (2015), [arXiv:1506.00013 [astro-ph.HE]].
- [27] M. Ackermann *et al.* [Fermi-LAT Collaboration], “Searching for Dark Matter Annihilation from Milky Way Dwarf Spheroidal Galaxies with Six Years of Fermi Large Area Telescope Data,” *Phys. Rev. Lett.* **115**, no. 23, 231301 (2015), [arXiv:1503.02641 [astro-ph.HE]].
- [28] A. Abramowski *et al.* [H.E.S.S. Collaboration], “Search for Photon-Linelike Signatures from Dark Matter Annihilations with H.E.S.S.,” *Phys. Rev. Lett.* **110**, 041301 (2013), [arXiv:1301.1173 [astro-ph.HE]].
- [29] G. Aad *et al.* [ATLAS], “Combined measurements of Higgs boson production and decay using up to 80 fb⁻¹ of proton-proton collision data at $\sqrt{s} = 13$ TeV collected with the ATLAS experiment,” *Phys. Rev. D* **101**, no.1, 012002 (2020), [arXiv:1909.02845 [hep-ex]].
- [30] A. M. Sirunyan *et al.* [CMS], “Combined measurements of Higgs boson couplings in proton-proton collisions at $\sqrt{s} = 13$ TeV,” *Eur. Phys. J. C* **79**, no.5, 421 (2019), [arXiv:1809.10733 [hep-ex]].
- [31] S. Schael *et al.* [ALEPH, DELPHI, L3, OPAL, SLD, LEP Electroweak Working Group, SLD Electroweak Group and SLD Heavy Flavour Group], “Precision electroweak measurements on the Z resonance,” *Phys. Rept.* **427**, 257-454 (2006), [arXiv:hep-ex/0509008 [hep-ex]].
- [32] G. Aad *et al.* [ATLAS and CMS Collaborations], “Measurements of the Higgs boson production and decay rates and constraints on its couplings from a combined ATLAS and CMS analysis of the LHC pp collision data at $\sqrt{s} = 7$ and 8 TeV,” *JHEP* **1608**, 045 (2016), [arXiv:1606.02266 [hep-ex]].
- [33] A. Alloul, *et al.*, “FeynRules 2.0 - A complete toolbox for tree-level phenomenology,” *Comput. Phys. Commun.* **185**, 2250 (2014), [arXiv:1310.1921 [hep-ph]].

- [34] J. Alwall *et al.*, “The automated computation of tree-level and next-to-leading order differential cross sections, and their matching to parton shower simulations,” JHEP **1407**, 079 (2014), [arXiv:1405.0301 [hep-ph]].
- [35] T. Sjostrand, S. Mrenna and P. Z. Skands, “PYTHIA 6.4 Physics and Manual,” JHEP **0605**, 026 (2006), [hep-ph/0603175].
- [36] J. de Favereau *et al.* [DELPHES 3 Collaboration], “DELPHES 3, A modular framework for fast simulation of a generic collider experiment,” JHEP **1402**, 057 (2014), [arXiv:1307.6346 [hep-ex]].
- [37] A. Djouadi, O. Lebedev, Y. Mambrini and J. Quevillon, “Implications of LHC searches for Higgs–portal dark matter,” Phys. Lett. B **709**, 65 (2012), [arXiv:1112.3299 [hep-ph]].
- [38] A. Djouadi, A. Falkowski, Y. Mambrini and J. Quevillon, “Direct Detection of Higgs-Portal Dark Matter at the LHC,” Eur. Phys. J. C **73** (2013) 2455, [arXiv:1205.3169 [hep-ph]].
- [39] H. Han, J. M. Yang, Y. Zhang and S. Zheng, “Collider Signatures of Higgs-portal Scalar Dark Matter,” Phys. Lett. B **756**, 109–112 (2016), [arXiv:1601.06232 [hep-ph]].
- [40] A. M. Sirunyan *et al.* [CMS], “Search for invisible decays of a Higgs boson produced through vector boson fusion in proton-proton collisions at $\sqrt{s} = 13$ TeV,” Phys. Lett. B **793**, 520–551 (2019), [arXiv:1809.05937 [hep-ex]].
- [41] A. M. Sirunyan *et al.* [CMS], “Search for dark matter and unparticles in events with a Z boson and missing transverse momentum in proton-proton collisions at $\sqrt{s} = 13$ TeV,” JHEP **03**, 061 (2017), [arXiv:1701.02042 [hep-ex]].
- [42] [ATLAS], “Search for new phenomena with top quark pairs in final states with one lepton, jets, and missing transverse momentum in pp collisions at $\sqrt{s} = 13$ TeV with the ATLAS detector,” ATLAS-CONF-2020-003.